Contract/Grant Number AFSOR 73-2541

INFLUENCE OF VARIOUS PARAMETERS ON INITIATION, STABILITY AND LIMITS OF DETONATIONS

W. Jost/ H. Gg. Wagner
Institute of Physical Chemistry
University
Göttingen, W. Germany

31 July 1978

Final Scientific Report, 73 June 01 - 78 July 31

Approved for public release; distribution unlimited.

Prepared for USAF Office of Scientific Research
Building 410, AFB D.C. 20332

and

EUROPEAN OFFICE OF AEROSPACE RESEARCH AND DEVELOPMENT
London, England

UNCLASSIFIED

SECURITY CLASSIFICATION OF THIS PAGE (When Data Entered)

REPORT DOCUMENTATION PAGE	READ INSTRUCTIONS BEFORE COMPLETING FORM
1. REPORT NUMBER: AFOSR-TR-79-0539	2. GOVT ACCESSION NO. / 3. RECIPIENT'S CATALOG NUMBER
4. TITLE (and Subtitle): INFLUENCE OF VARIOUS PARAMETERS ON INITIATION STABILITY AND LIMITS OF DETONATIONS	5. TYPE OF REPORT & PERIOD COVERED: FINAL Rept. 1 Jun 73 — 31 Jul 78 / 6. PERFORMING ORG. REPORT NUMBER
7. AUTHOR(s): W. JOST, R. GG. WAGNER	8. CONTRACT OR GRANT NUMBER(s): AFOSR-73-2541
9. PERFORMING ORGANIZATION NAME AND ADDRESS: UNIVERSITY OF GÖTTINGEN, INSTITUTE OF PHYSICAL CHEMISTRY, TAMMANSTR. 6, 34 GÖTTINGEN, FED REP OF GERMANY	10. PROGRAM ELEMENT, PROJECT, TASK AREA & WORK UNIT NUMBERS: 2308 / A2, 61102F
11. CONTROLLING OFFICE NAME AND ADDRESS: AIR FORCE OFFICE OF SCIENTIFIC RESEARCH/NA, BLDG 410, BOLLING AIR FORCE BASE, D C 20332	12. REPORT DATE: July 1978 / 13. NUMBER OF PAGES: 40
14. MONITORING AGENCY NAME & ADDRESS (if different from Controlling Office): 41p.	15. SECURITY CLASS. (of this report): UNCLASSIFIED / 15a. DECLASSIFICATION/DOWNGRADING SCHEDULE

16. DISTRIBUTION STATEMENT (of this Report)

Approved for public release; distribution unlimited.

17. DISTRIBUTION STATEMENT (of the abstract entered in Block 20, if different from Report)

18. SUPPLEMENTARY NOTES

19. KEY WORDS (Continue on reverse side if necessary and identify by block number)

ACCELERATION OF SPHERICAL FLAMES
INFLUENCE OF ORIFICES IN THE FLAME PATH

20. ABSTRACT (Continue on reverse side if necessary and identify by block number)

During this grant study was carried out on the mechanisms and processes governing transition between flame and detonation in unconfined spherical explosive clouds and how they can be influenced. During the last several years, emphasis has been on investigation of the influence of obstacles on flames and initiation of detonations. Experiments were performed in tubes of various diameters with an orifice placed in the flame plath. Various fuels (eg, hydrogen, methane, ethylene, acetylene and carbon disulfide) were used in stoichiometric fuel-oxygen mixtures with reduced nitrogen concentration (compared to air). Smear camera photographs

DD FORM 1473

401543

and simultaneously time resolved pressure records were taken. The orifices were found to cause very pronounced local accelerations together with a pressure rise when the flame is transmitted through the orifices. These effects were correlated with the open diameter of the orifices. The maximum pressure was obtained when the orifice diameter is about half the diameter of the initiation section. No detonations were observed in experiments with hydrocarbon-air mixtures.

INFLUENCE OF OBSTACLES ON THE PROPAGATION OF HYDROCARBON FLAMES

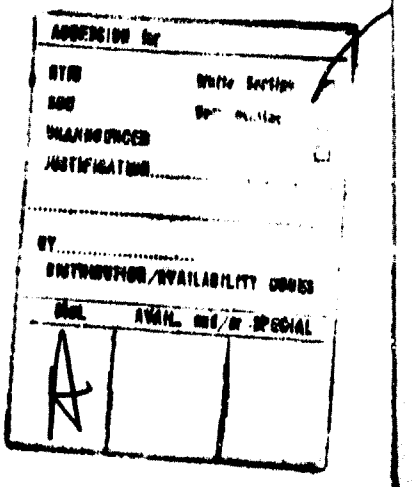

INTRODUCTION

The speed of a flame relative to the unburned gas is strongly influenced by turbulence in the unburned gas.

In an excellent review on turbulent combustion, Bradley (Andrews et al., 1975) indicated that there exists a linear relation between the turbulent flame speed and the Reynolds number $Re_\lambda = u' \lambda / \nu$, based on λ, the Taylor microscale and u' the fluctuation velocity. This relation seems to hold true for various mixture compositions (as long as Re_λ is above a certain critical value).

Somewhat different correlations are obtained by Ballal and Lefebvre (1975) who investigated stationary propane air flames in a combustion chamber at the entrance of which various nets were mounted for the generation of turbulence. At flow velocities up to 70 m/sec, turbulence intensities up to 15% could be reached. They found that at low turbulence intensity the thickness of the flame front is below L, the integral scale of turbulence. Here turbulence just increases the flame area by wrinkling the flame front. With an increasing intensity of turbulence, the flame front starts to become flat and finally a large part of the energy of turbulence is expended in the production of small eddies at the flame front. The thickness of the flame front is now larger than L. (For large systems additional effects due to large scale turbulence have to be considered).

A strong increase in the propagation velocity of self propagating flames by grids mounted in a tube has also been observed by Evans et al. (1949).

These experiments, together with numerous results obtained for burner flames, indicate a strong promoting influence of the intensity in turbulence on the propagation velocity of premixed flames. In his review on turbulent burning, Bradley points out that it is essentially the small scale part of the turbulence which is responsible for that effect.

Experimental studies of the development of detonation in tubes also showed that the acceleration of the flames is due to turbulence generated by the flow of the unburned gas ahead of the

flame. In fact, there exists a direct relation between the initiation distance and the initiation time of detonation in a tube and the Reynolds number $Re_d = V \cdot d/\nu$ of the flow in the unburned gas. The fact that inserting a short wire helix in the tube has a strong influence on the development of detonation (the so-called Shchelkin spiral) has been known (and used) for a long time. A piece of bent wire 10 cm long, placed obliquely to the axis of the tube, can reduce the initiation distance of detonation by a factor of ten, corresponding to the Reynolds number Re_d of several hundred thousand. In this case however, as with the Shchelkin spiral, other effects become important, favoring the build-up of pressure waves. When the flow passes the wire, an area of stagnant flow is formed behind the wire, acting as a pocket of (partly) unburned gas surrounded by the flame or burned gas causing it to burn concentrically. If the pressure in the unburned gas is already sufficiently high, this can actually lead to an explosion giving rise to detonation (Schüller, 1954). Details of this phenomenon have been photographed during the development of detonation in constant area tubes by Oppenheim et al. (1969).

In the case of spherical flames, the influence of turbulence should be essentially the same as in burner flames or in flames propagating through tubes (see e.g. Khitrin, 1962) and the arguments of Bradley must be applicable under such circumstances as well. As far as the development of detonation is concerned, the situation in spherical geometry is completely different than that in tubes of constant cross-section area because there is no wall available for the generation of turbulence in the unburned gas. Soap bubble experiments ($d \leq 15$ cm), which were performed in a way that no reflected waves could come back to the flame, did not show acceleration of the flame, even for C_2H_2-O_2 mixtures, as long as weak ignition was used. Experiments of Lee (Bach et al., 1971) do show however that in C_2H_2-O_2 mixtures the ignition energy for the immediate establishment of a spherical detonation is quite low.

A fundamental question in this respect is what is the basic nature of the effects that can cause acceleration of premixed spherical flames? There is flame induced turbulence which can start by the formation of polyhedral flame fronts. The existence of this effect in spherical flames has been observed by Troshin and Shchelkin (1955; 1963) and treated theoretically by Istratov and Librowich (1969) on the basis of Markstein's model. Taylor instabilities can also give rise to flame acceleration. These effects should become more important for combustible clouds of larger size. Other effects that produce disturbances upsetting the symmetry of the flame, such as buoyancy or sound wave reflections, can also cause flame acceleration by triggering the onset of their polyhedral structure.

The situation is somewhat different in clouds with inhomogeneous mixture distribution or in clouds with internal flow or turbulence. Here the flame front is essentially non-symmetric, having large scale wrinkling or being separated into different domains of burning throughout the space. In addition, some particular gasdynamic effects have to be taken into consideration, especially with respect to their influence on the increase of the effective flame front area over that of a smooth surface. This affects the rate of the evolution of exothermic energy, the exothermic power which can be considered as equal to the product $\alpha \Lambda$, where Λ is the local laminar flame speed while α is a factor expressing the influence of turbulence, and the real total flame area $F(t)$ at time t. The ratio of $F(t)$, the real flame area, to the corresponding spherical surface area, $4\pi(\bar{r}(t))^2$, can also be considered as a function of the size of the cloud.

If one wants to represent the heat release rate in such a cloud by a spherical flame front, the effective flame speed is given by $(\alpha \cdot \Lambda \cdot F(t))$ as long as no autoignition processes occur as a consequence of some particular gasdynamic effects.

While the factor F(t) can be obtained only from models or from large scale experiments, the quantity α is directly measurable in laboratory experiments. Recent experiments of D. Bradley and co-workers do indicate the range over which α can vary, including conditions under which turbulence is generated by external sources. In this connection there arises a question of how large can α become if the energy for the generation of turbulence is provided by the burning gas itself.

A relatively simple way to generate a well defined scale of turbulence is by means of grids. In order to avoid the influence of additional wall turbulence, either grids in spherical or hemispherical system, have to be used for the measurement of the parameters.

EXPERIMENTAL ARRANGEMENT

A cubic container is made gas-tight by thin transparent paper walls. Its bottom is a metal plate with an ignition source in the middle. Pressure sensors are placed at different distances from the spark gap. Semispherical grids can be mounted on the bottom plate (Fig. 1).

The container is filled with a premixed hydrocarbon-oxygen-nitrogen mixture by passing it through into open air. Proper chechs were made to insure that the concentration of the out-flowing gas was the same as that of the inflowing mixture.

Just before each test, the paper walls were ruptured and the gas flow stopped. Then the gas mixture was ignited by a weak spark. The propagation of the flame front could be observed by means of a torating drum-camera mounted in such a position that the trace of the propagating flame could be recorded at the middle of the container.

Experiments were also performed with ignition in the middle of the container. In these cases, spherically shaped wire screens were mounted concentrically around the ignition source. The Specifications of the wire screens in our experi-

ments are listed in Table 1.

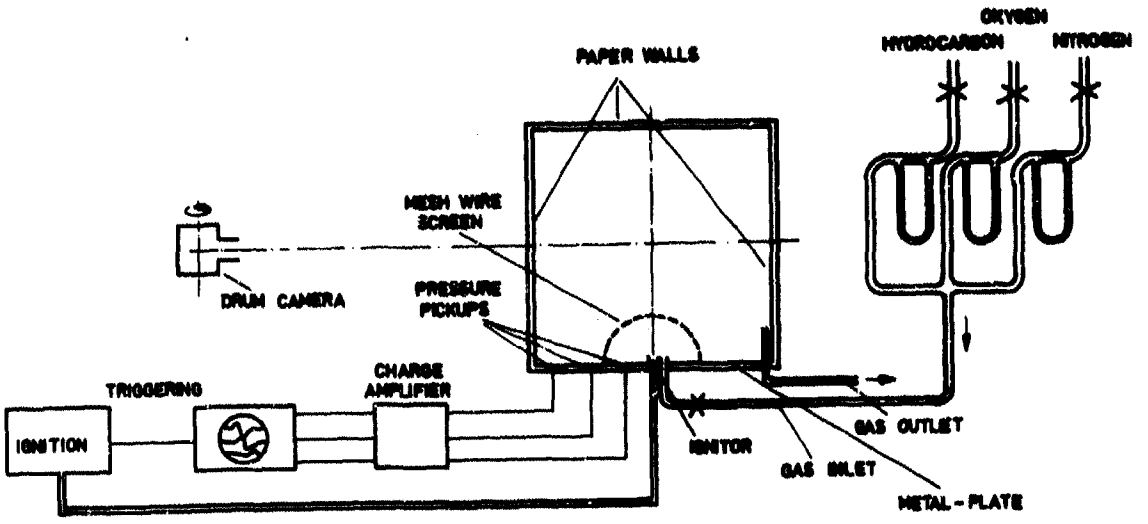

Fig. 1: Experimental arrangement

Table 1: Specification of wire Screens

diameter of the grids cm	mesh size l mm	wire diameter d mm
9, 14, 18	1.6	0.8
9, 14, 18	2.8	0.8
9, 18	3	0.5
9, 18	6.3	2
9	6.3	0.8
9	3	1.5
9	1	0.2
9	6.3	1.4
9	10	1.8
9	16	1.8
9	5	1.8
9	3	1.5
9, 14, 18, 36	1.5	0.25

EXPERIMENTAL RESULTS

For mixtures with air as oxidizer and without a wire screen, the time resolved streak records show only a line inclined at an angle φ_1 with respect to the direction of the film motion. This indicates, of course, a constant velocity of flame propagation in the mixture after ignition. The flame velocities V obtained from these records fit quite well the values of laminar flames in the literature, calculated by taking into account the continuity relation $V = \Lambda(\rho_0/\rho_1)$, where ρ_1 and ρ_0 are the densities of the mixture before and behind the flame front, respectively.

When a wire screen is used, the drum camera pictures show at first the same angle, φ_1, as in the experiments described above, but immediately after passing across the screen, the angle increases to φ_2. The ratio $\varphi_2/\varphi_1 = \alpha$ gives the value of the factor expressing the change in speed caused by the wire screen without any external influence. Thus one has:

$$\alpha = \frac{V_{outside}}{V_{inside}} .$$

Experiments with screens of various radii, r, were carried out. The smallest had a diameter of 2r = 9 cm. The largest was a semispherical screen of 36 cm dia. No striking dependence in measured values of α on the overall diameter of the screen was noticed.

In order to examine further the influence of the size of the experimental system, especially to exclude the possibility of some disturbances that could have been caused by the thin paper walls that were ruptured before each test, a container 8 times larger than that used for our main experiments was employed. Its size was 60 x 60 x 60 cm. This yielded exactly the same results as those obtained before. One may thus conclude the paper wall did not cause any disturbance that could invalidate our experimental results. The only conclusion one can reach is

that it was solely the turbulence generated by the wire screen that caused the flame propagation speed to augment. Turbulence shows no dependence on the size of the experimental system, i.e. it is independent of the radius r of the wire screens used or of the volume of combustible cloud.

The experiments showed that the essential factors influencing the value of the parameter α are the laminar flame speed Λ_L, the mesh size l of the grid and the diameter d of the wire. As diameter of the wire is increased, the augmentation of the flame propagation speed induced by the grid becomes larger. If the wire diameter is held constant, the value of α increases when grids of smaller mesh size are used. When l is too small, the flame is quenched.

In order to obtain information on the influence of Λ_L on α, stoichiometric mixtures of different hydrocarbons with air were used. As expected, a definite dependence of the speed augmentation factor α on Λ_L was thus observed. At the same conditions (e.g. for the same grids), the flame propagation speed in stoichiometric acetylene-air mixture is augmented more than that in the stoichiometric ethylene-air which, in turn, exceeds that exhibited in the stoichiometric propane-air. In general then:

$$\alpha = \alpha(\Lambda_L, d, l).$$

For low laminar flame speeds (propane-air, methane-air) with grids made from thin wires, the screen does not influence the flame at all, i.e. $\alpha = 1$. Apparently these flames do not generate enough turbulence at the grid to enhance propagation velocity.

If one evaluates the Reynolds number on the basis of the wire diameter and the flow velocity w_N of the unburned gas ahead of the flame at the moment when the flame reaches the screen, $W_N = \Lambda_L [(\rho_0/\rho_1) - 1]$, then one finds that α remains one until the Reynolds number is increased to about 60 or 70. For $Re_{W_N} < 60$ no augmentation in flame speed is observed. For $Re_{W_N} > 70$ the

factor α increases strongly as the Reynolds number becomes larger. Moreover the value of α increases more for smaller mesh sizes and less for larger sizes.

In order to check the influence of Λ still further, propane-air mixtures with so much oxygen added that the laminar flame velocity was 80 cm/sec were also used. This yielded the same results as those of the C_2H_4-air mixtures with Λ = 80 cm/sec. Values for flame velocities between those of C_2H_4-air and C_2H_2-air were also obtained by adding O_2 to the C_2H_4-air mixture.

Flame outside the wire screen usually exhibited constant flame velocity over some distance in spite of the fact that the Reynolds number Re_W in the volume elements some distance away from the grid decreases because the flow velocity of a volume element passing through the grid at time t is lower than for that passing at the instant t + Δt. This throws some doubt on the validity of using Re_W as the correct parameter for the representation of experimental results.

Nevertheless in Fig. 2 the data are represented in form of a plott of α as a function of Re_W with the mesh size as a parameter. It is apparent that for high values of Re_W the dependence of α on the Reynolds number becomes very small, especially for fine grids.

This Reynolds number refers to a special situation and it seems usefull to relate the data to a Reynolds number based on more general properties. Bradley et al. obtained good correlations of available turbulent flame speeds on the basis of a Reynolds number, which contains the Taylor length λ as a characteristic property. The turbulent Reynolds number based on the Taylor microscale λ appears to be able to correlate the experimental data from widely different turbulent situations and geometry.

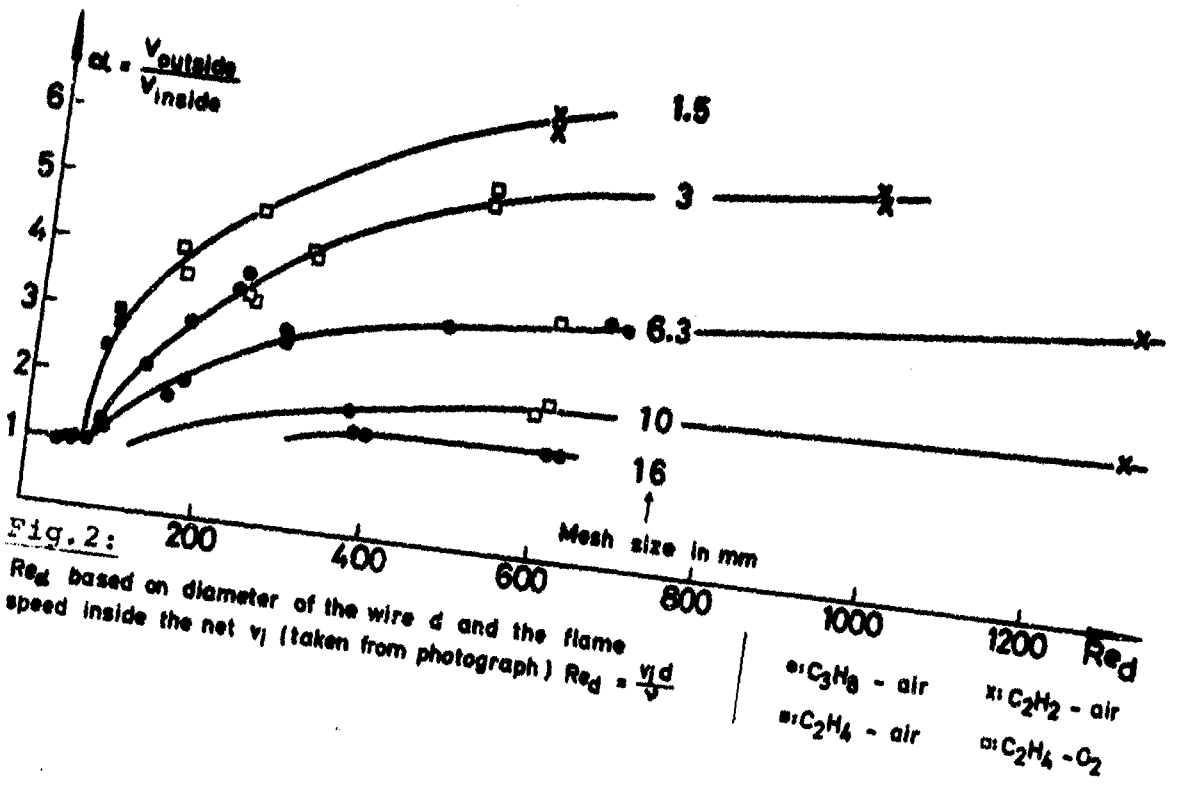

Fig.2: Re_d based on diameter of the wire d and the flame speed inside the net v_l (taken from photograph) $Re_d = \frac{v_l d}{\nu}$

The various data of the turbulent flame velocity ratio $\alpha = \frac{V_o}{V_i}$ appears to be directly proportional to the turbulent Reynolds number (Re_λ) itself over the range of $Re_\lambda \leq 400$. Based on such a simple linear dependence we could perhaps extrapolate to the required value of α and see if the corresponding value of Re_λ can be met in these turbulent flames. Above, the value of α is correlated with the Reynolds number based on the flow velocity $W_n = \lambda(\frac{\rho_o}{\rho_1} - 1)$ of the unburned gas and the characteristic length used is the wire diameter of the screen. Since these results are obtained for self-propagating transient flames, they differ from those experimental situations where the turbulence in the stream can be controlled independently, it would be of interest to see if our data come under the $\alpha - Re_\lambda$ correlation of Bradley et al. Turbulence immediately behind the spherical wire screen is not homogeneous. It is nevertheless possible to measure mean values of the velocity fluctuation u' at various positions behind the grids. These measurements (performed by Dr. Herbeck)

indicate the following: If u' is measured over a certain distance above the grid and the probe is shifted parallel to the surface of the grid, than u' remains constant if the distance from the grid is larger than ten times the mesh size. For shorter distances however u' varies when the probe is moved parallel to the grid, u' shows a minimum above the centers of the mesh (here turbulence starts at larger distances from the grid than above the wires) and a maximum somewhere between the center of the mesh and the middle of the wire.

Some results for u' as a function of the local flow velocity are shown in Figure 3 for two different grids, taken at distance of 0.5 cm and 1.7 cm above the grid.

For a given grid the degree of turbulence $I_t = \frac{u'}{u}$ (u = local flow velocity) is nearly independent of the flow velocity u $\frac{dI}{du} = 0$ and it decreases with increasing distance from the grid.

For grids very efficient with respect to flame acceleration, I_t may be larger than 0.2 close to the grid whilst for the less efficient grids it is closer to 0.1. For grids with larger mesh sizes I_t is much smaller close to the grid.

As a rough approximation we can assume the turbulence intensity $u' = \sqrt{u^2}$ to be a fixed fraction of the maximum flow velocity at the grid $W_n = \Lambda \left(\frac{\rho_0}{\rho_1} - 1 \right)$ with a value of $I \approx 0.1$.

The region close to the grid is, as mentioned above, not isotropic. However, in determing the turbulent flame velocity ratio α from the experimental streak record, the average flame speed after the grid has been used. Therefore α, to a certain degree combines the "near field" and the "far field" flame velocity. Sufficiently far downstream of the grid the turbulent flow may be taken to be isotropic at least for efficient grids although in the case of spherical diverging transient flow, this may not

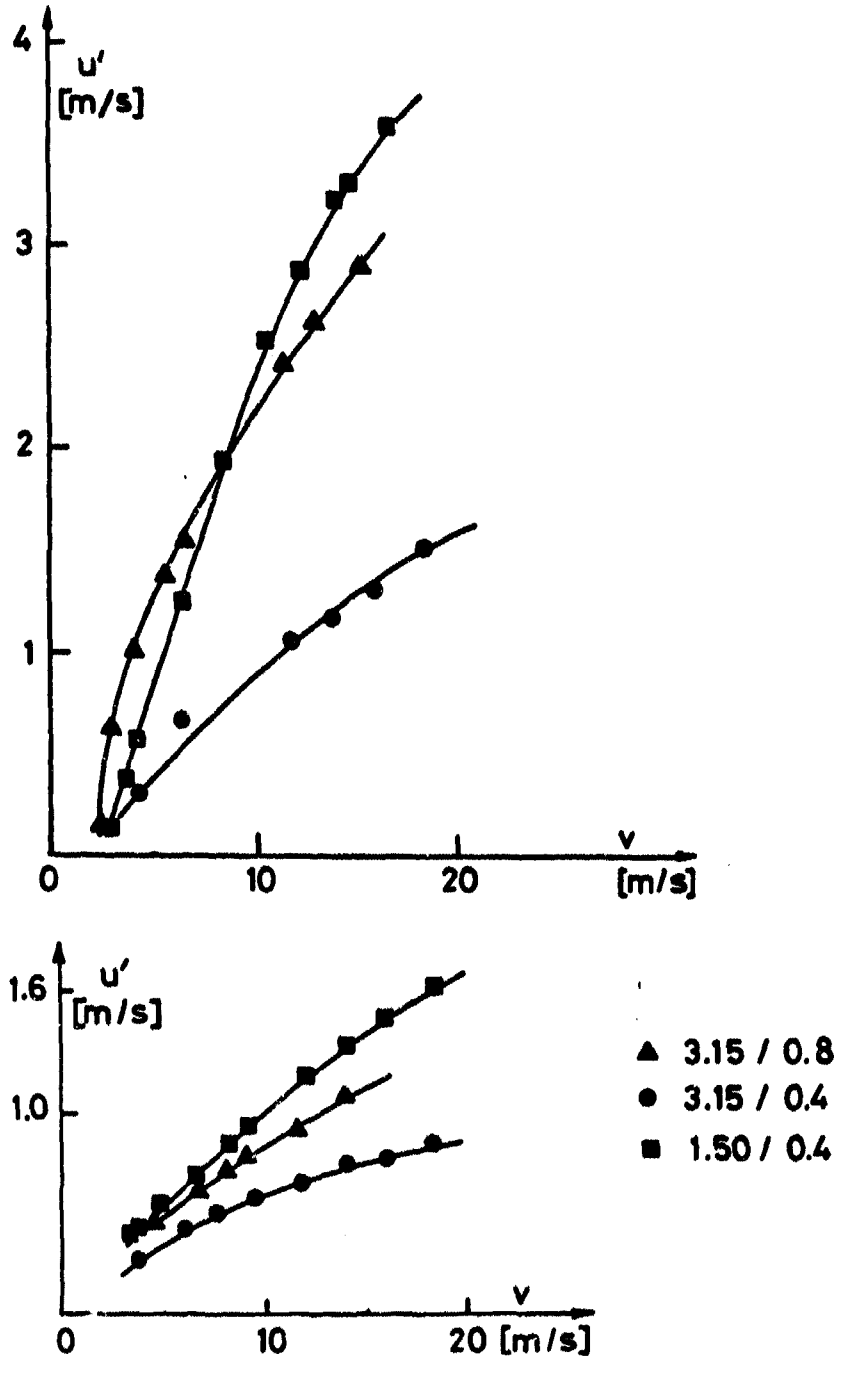

Fig. 3: Velocity fluctuations u' behind grids

necessarily be the case. Assuming isotropic turbulence the Taylor microscale can be computed using the empirical formula given by Dryden.

$$\lambda = \sqrt{48.64 \frac{\nu d}{u'}}$$

The turbulent Reynoldsnumber Re_λ can be written as

$$Re_\lambda = \frac{u' \cdot \lambda}{\nu} = \sqrt{\frac{48.64\ u' \cdot d}{\nu}} \approx Re_1^{1/2}$$

$$Re_d = \frac{u'\ d}{\nu} \quad , \quad Re_w = \frac{u' \cdot d}{\nu}$$

If we choose $I \approx 0.1$ and d as the wire diameter of the screen the above expression yields

$$Re_\lambda \approx 2\ 2\ Re_w^{1/2} \qquad 1$$

where Re_w is the wire Reynoldsnumber used in correlating α. The results for α range from about 1 to 6 for a range of $70 < Re_w < 600$ for hydrocarbon-air mixtures. In terms of Re_λ, using Eq. 1, the corresponding range of Re_λ is $20 < Re_\lambda < 50$. These data fall within the correlation of Andrew et al. quite well. For oxygen enriched mixtures, the range of Reynolds number has been measured $Re_w \leq 4000$. However, the value of α is only slightly larger than for the corresponding hydrocarbon-air case (i.e. $\alpha \sim 6$). Using Eq. 1 to reduce the Re_w for the oxygen enriched cases, we obtained $Re_\lambda \leq 120$ for an assumed $I \approx 0.1$. Again the oxygen enriched data falls into the Bradley correlation. Thus it appears that in the case of transient free propagating spherical turbulent flames the turbulent Reynolds number Re_λ appears to provide an adequate parameter for correlation. The values of Re_λ that can be achieved in these experiments by the system itself are therefore rather low. Since Re_λ is proportional to the square root of the product of u' and d a hundred fold increase in u'd would only raise the value of Re_λ by an order of magnitude. For hydrocarbon-air mixtures where the flow

velocity $u = \lambda \left(\frac{\rho_o}{\rho_1} - 1 \right)$ is limited even for a turbulent flame, a thousand fold increase in the characteristic length scale λ would be required to obtain the necessary high turbulent Reynolds number Re_λ. Thus on a very large scale, it may be possible to achieve a high flame speed. The range for such an extrapolation to large scale is limited however because the magnitude of λ will by far exceed the characteristic length of the flame zone. Therefore other means will have to be taken in order to increase Re_λ. One of these could be turbulence generated artifically by other sources than the flame. Here, however, the decay time of turbulence after its generation limits the effect on the flame speed. Another possibility is the generation of higher values of u'. This will be treated in the next chapter on the influence of orifices in the flame path.

In order to find whether the propagation velocity of hydrocarbon-air flames can be augmented further, two and three screens were mounted one over the other (9, 14, 18 cm). The acceleration of the flames at the first screen were essentially the same as in Fig. 2. At the second screen the flame speed increased more, but the value of α_2 was smaller. At the third screen, the increase in flame velocity was very small, the corresponding value of α_3 being practically equal to one. The largest augmentation in flame velocity caused by three screens was $\alpha_{1,2,3} \approx 12$ for stoichiometric C_2H_2-air mixtures. There was no indication of an onset of detonation in these experiments with air mixtures in spite of the fact that the conditions for flame acceleration were very good due to the generation of fine scale turbulence by the screens we used.

It is certainly not clear how flame induced turbulence in an unconfined cloud could reach an intensity of turbulence comparable to that generated artificially by screens. Therefore in such clouds of hydrocarbon-air mixtures whose flame velocities

are $\Lambda \leq 100$ cm/sec one should expect the values of α to be considerably below that reported here for the C_2H_2-air system. Thus, as long as no particular gasdynamic effects occur, there is some safety margin for α before a situation similar to that observed by us in the C_2H_2-air mixture is reached.

FLAME SPEED AUGMENTATION WITH OXYGEN ENRICHED AIR

It has been shown that α is larger for hydrocarbon-air mixtures having higher flame velocity. There is an upper limit of Λ for hydrocarbon-air mixtures of about 1.6m/sec. In order to reach higher values of Λ, stoichiometric mixtures of C_2H_4 and C_2H_2 with O_2 were used with the addition of a certain amount of N_2. Earlier experiments with C_2H_4 and oxygen enriched air already indicated that α becomes larger when the N_2 content in stoichiometric mixtures is reduced. They did not show, however, whether this increase continues, in particular whether a maximum value of α is reached or whether the mixture starts to detonate below a certain level of N_2 content. These experiments were therefore continued with a drum camera of higher time resolution, while the container was fitted with a screen of 9 cm in diameter.

The experiments indicate that α may become still significantly larger in mixtures of higher laminar flame speed. If quantity α is plotted as a function of Λ for a grid of a fixed value of d and l, the curve shows the familiar shape leading asymptotically to an "effective upper bound" of α. However, further increase of Λ associated with a reduction of the N_2 content leads to the onset of detonation. The same mixtures showed no acceleration in experiments where no grids were placed in the flame path.

Results obtained in the course of these experiments are shown in Table 2.

The observations were made by measuring pressure at various positions and by recording the flame trace by the streak camera as before. In the case of detonation, velocities of about 3000 m/sec and pressures of over 10 bar were recorded. Unfortu-

Table 2: Correlation of data on the onset of detonation for for various grids as a function of the nitrogen content. (a) For ethylene mixtures; (b) for acetylene mixtures

C_2H_4

% N_2 \ grid $\frac{d}{mm}/\frac{l}{mm}$	0.8 / 6.3	0.8 / 2.8	1.5 / 3	0.8 / 2	2 grids 0.8 / 2.8
60					□
50		△			■
43		△		△	■
33		△ ○	○	▲	
29	○	▲ ●	●		
23	○				

detonation no detonation

grid diameter

9 cm	●	○
14 cm	▲	△
2 grids 9 / 14 cm	■	□

C_2H_2

% N_2 \ grid $\frac{d}{mm}/\frac{l}{mm}$	0.8 / 2.8	0.8 / 6.3
53	○	○
46	○	○
36	●	●

nately the luminosity of the detonations was so high that the trace of the flames inside the grid could not be clearly observed. We therefore cannot exclude that in these cases the flames inside the grids were already slightly accelerated.

Experiments using various mixtures of C_2H_4-O_2-N_2 and C_2H_2-O_2-N_2 did show, however, that for the onset of detonation this Reynolds number is not an essential parameter anymore.

In the experiments described above, it was shown that additional grids can further increase the value of α. It was therefore of interest to see whether the onset of detonation is also influenced by the use of additional screens. Preliminary tests revealed that is indeed the case. While for one screen of 9 cm in diameter, detonation in a C_2H_2-O_2-N_2 mixture started when the N_2 content was reduced to 30%, with the use of an additional screen (14 cm diam.) the N_2 content could be increased to as much as 50% before the onset of detonation was eventually deterred.

FLAME ACCELERATION BY OBSTACLES

The propagation of flames has been investigated in great detail over a very wide range of conditions. It has been realized that obstacles in the path of the flowing unburned gas can strongly increase the local flame velocity and cause pressure pulses which may lead to the initiation of a detonation in proper mixtures. A first detailed study of this effect has been performed by Wheeler and co-workers. They obtained very high flame velocities by mounting a set of 12 orifices in proper distance into a tube, open at both ends. For methane-air, the value of χ went up to 70 (for the whole device).

The mechanism of flame propagation through narrow channels has been investigated by Wolfhard et al.. A CH_4-air flame extinguishes when the width of the tube comes below a critical diameter. Nevertheless, the mixture downstream of the channel may ignite. This happens more often when channels of 10 mm length are used compared to shorter channels. Similar results have been obtained during numerous investigations of critical slit width for flame penetration. An agreement on a standart test equipment for this characteristic quantity has been achieved.

Another application of flames passing through channels happens in stratified charge engines (see Kumagui et al.). It has also been applied for the ignition of plane flames in large tubes (flame brush plate).

An important feature of these devices is the fact that they generate locally high levels of turbulence in the unburned gas. It therefore seemed usefull to investigate the influence of typical obstacles, for which the flow properties have been investigated in some detail. There are two types of obstacles which fulfil this requirement: rods and orifices. A detailed

description of the flow behind rods and orifices is given in Hinze's book: Turbulence. For reason of experimental simplicity most of our experiments have been performed with circular orifices.

EXPERIMENTAL SET UP

Figure 4 shows a schematic drawing of the experimental set up.

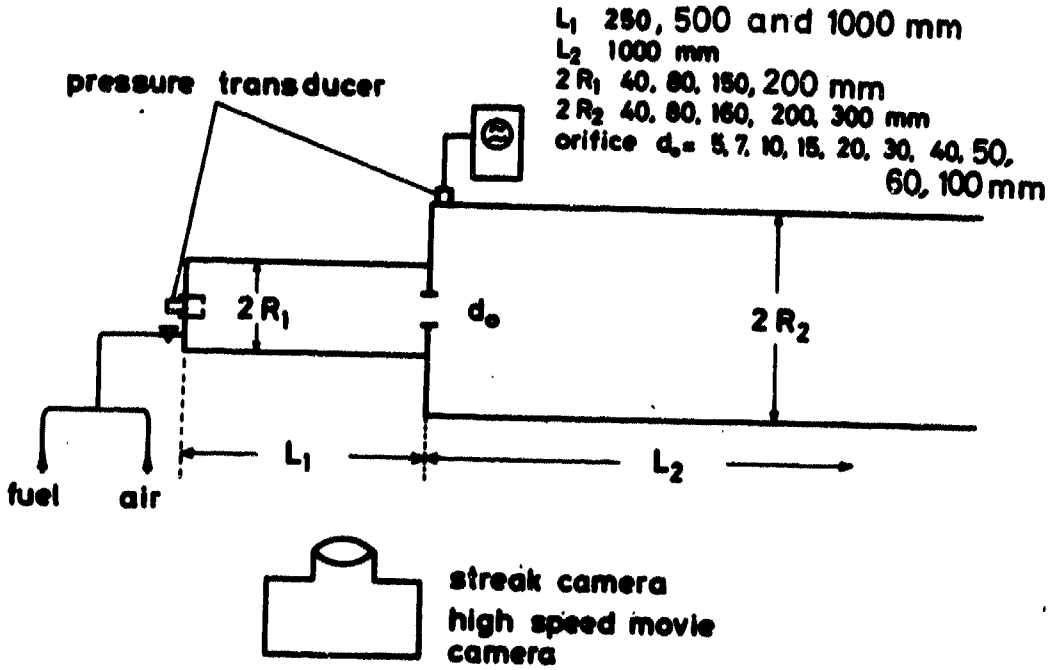

Fig. 4: Experimental set up

An ignition section is connected to a downstream tube. Between both orifice plates can be mounted. The ignition section is closed at one end. A spark gap is mounted at the closed end. Pressure gauges can be mounted at various positions. The one

end of the downstream tube is kept open during the experiment. For the registration of the flame propagation process, smear camera pictures as well as high speed film cameras (Lowcam. Fastax) have been used. The passage of the flame through the orifice could be checked by conductivity measurements with electrodes downstream of the orifice.

The dimensions of the tubes and the orifices in Fig. 4 are given in millimeter. A statement 40/160 means that the diameter of the ignition section was 40 mm, that of the downstream tube 160 mm. If not stated otherwise, the length of the ignition tube was L = 500 mm.

In most of the experiments stoichiometric C_2H_4-air mixtures have been used (in both tubes).

EXPERIMENTAL RESULTS

Photographic Investigations

For a smooth tube of the dimensions used in these experiments without obstacles and ignition at the closed end, C_2H_4-air flames accelerate slightly due to flame curvature and turbulence generated at the wall.

For comparison with the experiments with spherical grids, similar grids have been mounted as obstacles between the two tubes. On a smear camera picture one can observe that the flame speed is higher immediately downstream of the grid. One can calculate the acceleration factor

$$\alpha = \frac{V_{\text{behind grid}}}{V_{\text{ahead grid}}} = \frac{V_o}{V_i}$$

Some date for α are given in Tab. 3 for various types of grids and for various mixtures. The α values are close to those obtained with spherical grids.

Table 3: Flame acceleration at grids in tubes.
Mean values of α for various mixtures and grids

Grids ($^{l}/_{mm} \times {}^{d}/_{mm}$)	Mixtures C_2H_4/air	CS_2/air	$CS_2/O_2/50\%N_2$
1.6 x 0.71	3.8	4.0	2.6
3.15 x 0.56	4.7	4.1	3.0
3.15 x 0.8	4.9	4.1	3.3
3.15 x 1.12	3.9	3.7	4.9

Similar smear camera pictures are obtained if orifice plates are mounted between the two tubes instead of grids . One example is shown in Figure 5.

In order to check whether the shape of the orifice influences the process, a set of orifice plates, shown in Figure 6, has been tested. They all have the same total open area. On the film one observes that downstream of the orifice plate the flame accelerates slightly up to a maximum of the flame propagation speed a short distance downstream and than decelerates. Speeds taken from the slope of the luminous trace on the film are to a certain extend average quantities. Sometimes, processes running in or against the film speed direction cannot always be separated from processes along the tube axis. Nevertheless, these experiments show some general trends:

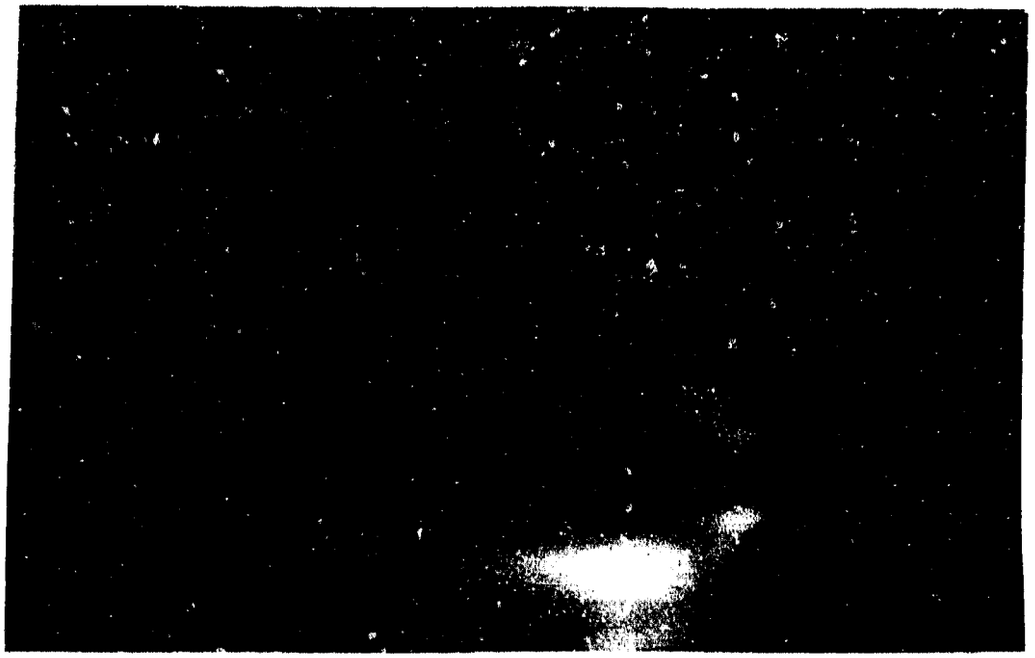

Fig. 5: Picture of a flame in a tube with an orifice plate as obstacle as taken by a rotating drum camera

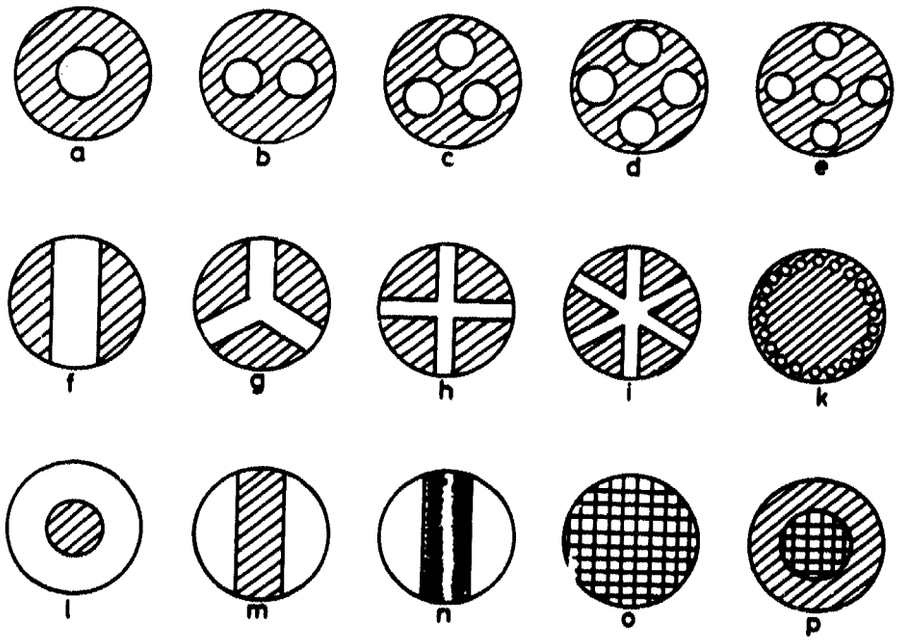

Fig. 6: Various orifices and obstacles

1.) In a zero approximation, the ratio of the flame speeds is independent of the shape of the orifices for all the orifices shown in Fig. 6. This holds even if a flat plate is mounted instead of a cylinder.

2.) A strong influence can be realized if the open area of the orifices is changed (for the same tube cross section). In the following, we will, therefore, use the ratio of open area F_o to total area of the tube F_g as a parameter for the representation of the results. This quantity F_o/F_g essentially determines speed and momentum of the jet and therefore the turbulence properties in the jet and its surrounding.

The following experiments have all been performed with orifices of circular cross section constructed after DIN rules for flow meter orifice plates. The smear camera pictures can roughly be divided into three groups:

1.) If the orifice is very small ($2r \leq 5$ mm somewhat depending on the shape of the orifice and the mixture), combustion does not proceed through the orifice, it is extinguished.

2.) If the orifice diameter is large (close to the tube diameter), the flame passes through the orifice as a flame tongue. The level of turbulence is somewhat increased by the orifices. Therefore, flame speed is slightly higher.

3.) For medium size orifices, this refers to the ratio F_o/F_g, the situation is more complex. On the film one observes that downstream of the orifice combustion starts some distance (X_i) away from the orifice. It seems to propagate into downstream and upstream direction (Fig. 7). The distance X_i can be measured directly on the film. (It depends slightly on the diameter $2R_2$ of the downstream tube).

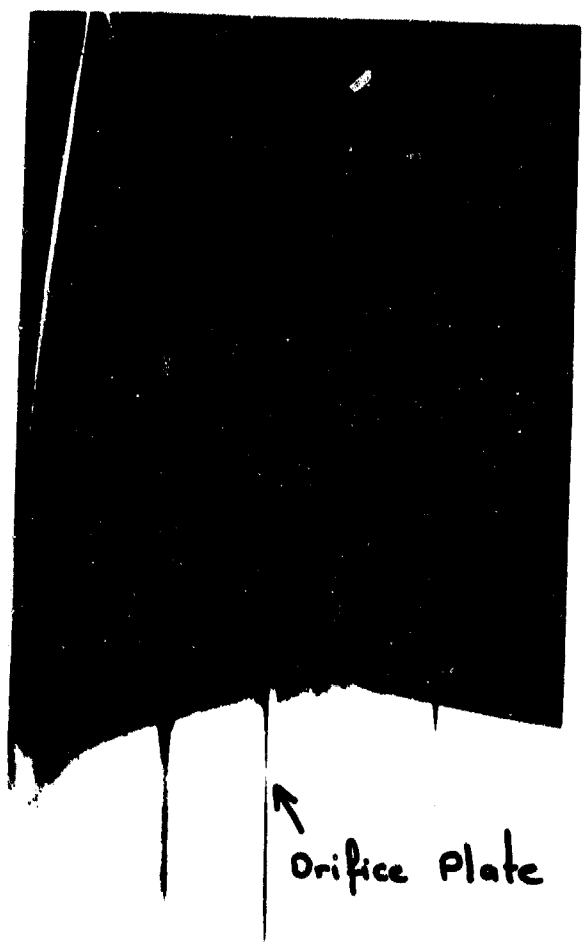

Fig. 7: Reignition at distance X_i downstream of orifice

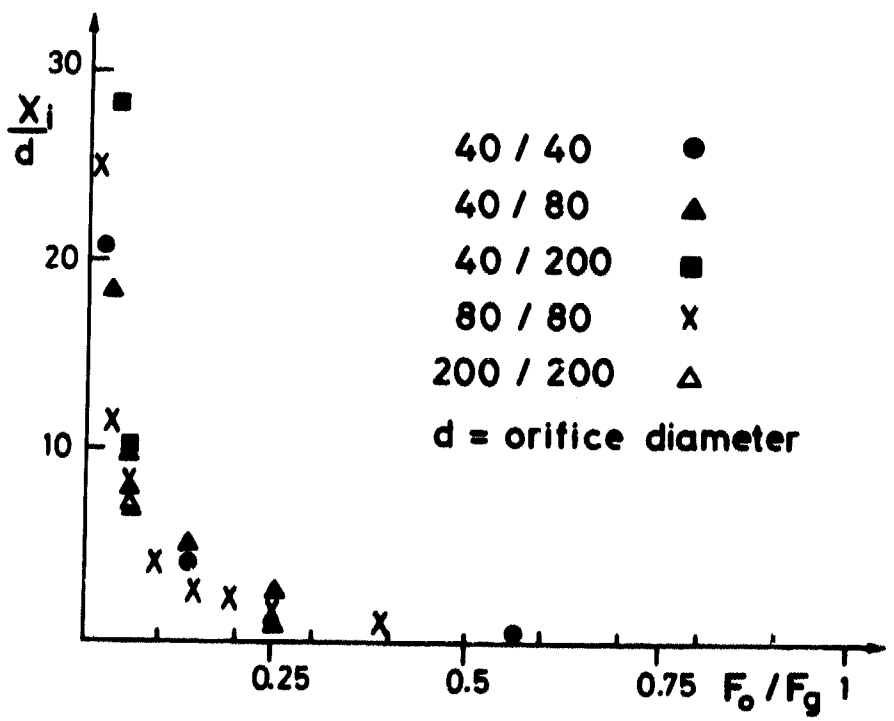

Fig. 8: Reignition distance X_i as a function of the area ratio F_o/F_g for various tube combinations

For driver sections with small diameters (40 and 80 mm) these values of X_i are reasonably well defined. They are plotted as X_i/d (d = orifice diameter) in Figure 8 for various tube combinations (diameter of upstream and downstream tube) as a function of F_o/F_g. It is obvious, that towards small F_o/F_g X_i increases strongly until the flame fails (case 1), while towards large values of F_o/F_g the X_i become small because the flame penetrates directly (case 2).

These phenomena can be quite well observed on high speed movie - Figure 9 -(taken with a Fastax camera).

After the flame reached the orifice plate it seems to extinguish. Some time later it looks as if reignition takes place and a flame kernel expands spherically with very high speed while the center of the kernel moves away from the orifice, approximately with jet speed. The subsequent events observable on the film are very interesting but rather complicated and shall not be discussed here.

For tubes of larger diameters, the reignition becomes more complicated. This can be realized in Figure 10 which shows the "reignition" from a 20 cm diameter upstream tube and a 50 mm diameter orifice (observed through a 2 cm wide slit). From various reignition centers or surviving flame kernels, flames propagate and finally merge. A flame velocity in downstream direction of about 500 m/sec results.

The situation for a 100 mm orifice (and the same upstream tube F_o/F_g = 0.25) is demonstrated in Figure 11. Even in this case the flame front does not penetrate as a smooth area and the flame velocity is around 450 m/sec.

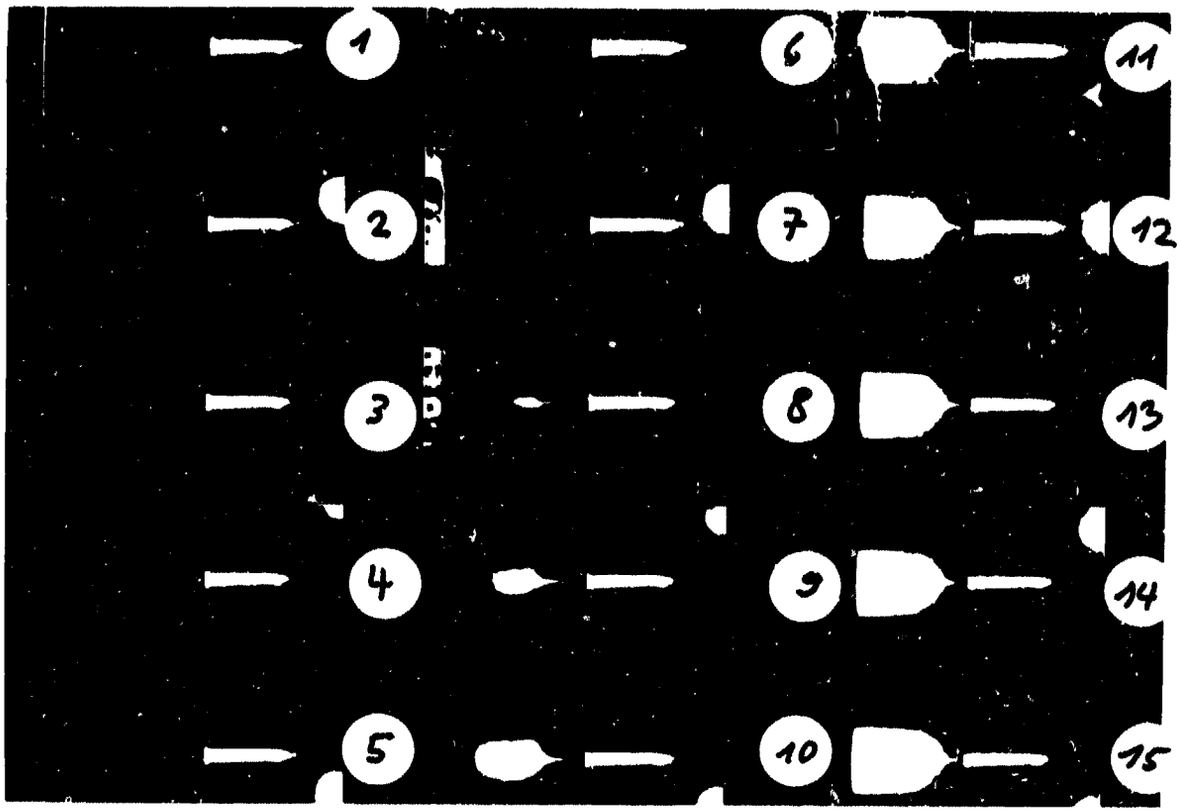

Fig. 9: Reignition downstream of orifice taken with a Fastax Camera (3000 frames per sec). Flame arrives at orifice in Picture No. 1. Begin of reignition becomes visible in No. 6.

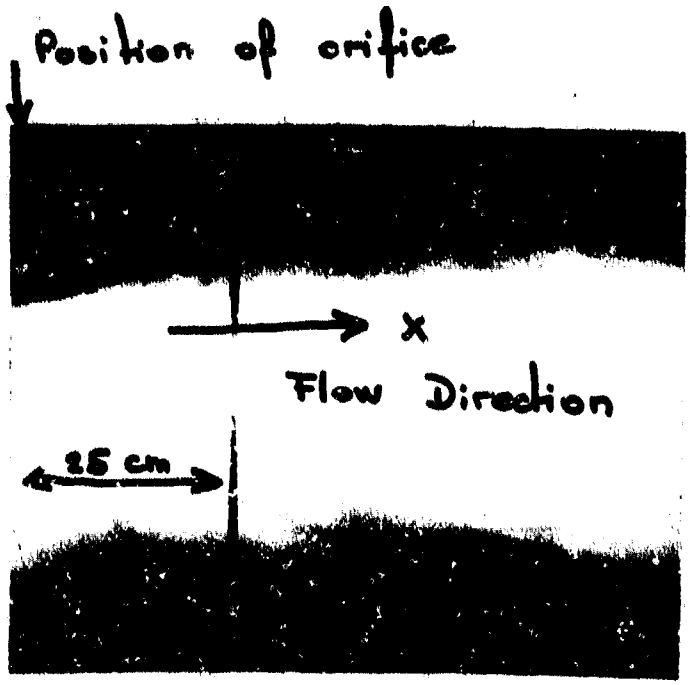

Fig. 10: Smear camera picture of flame passage through a 10 cm diameter orifice for tube combination 200/200

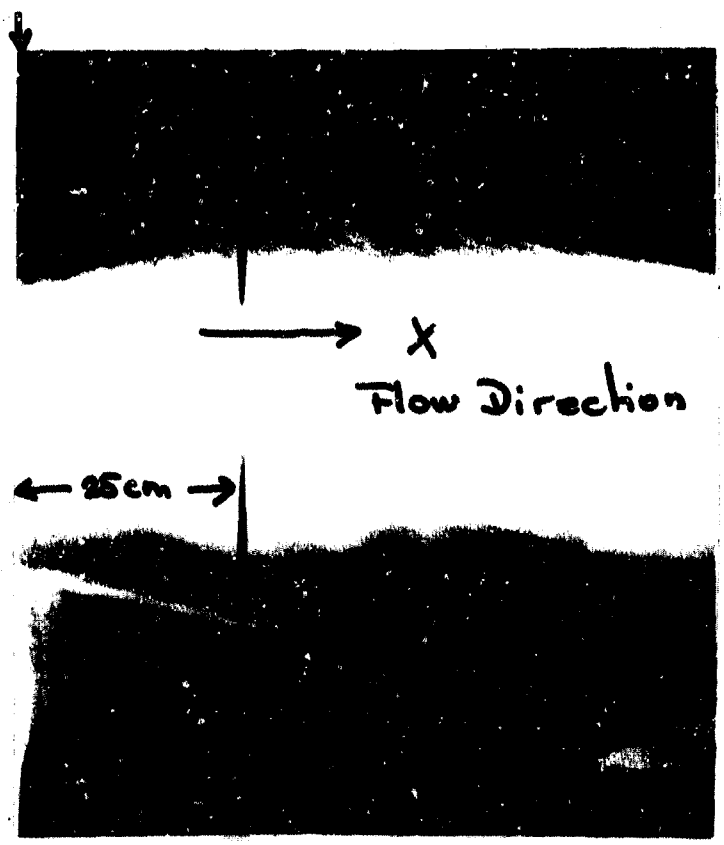

Fig. 11: Smear camera picture of flame passage through a 5 cm diameter orifice for tube combination 200/200

FLAME VELOCITIES BEHIND ORIFICES

On the smear camera pictures the increase of the flame speed downstream of the orifice can be approximately divided into two parts. A certain value is obtained shortly after the orifice (V_2) which increases somewhat some distance further downstream (V_3). In the ignition section the propagation speed of the flame increases continuously. The results for C_2H_4-air, stoichiometric in 80 mm diameter tubes are shown in Figure 12.

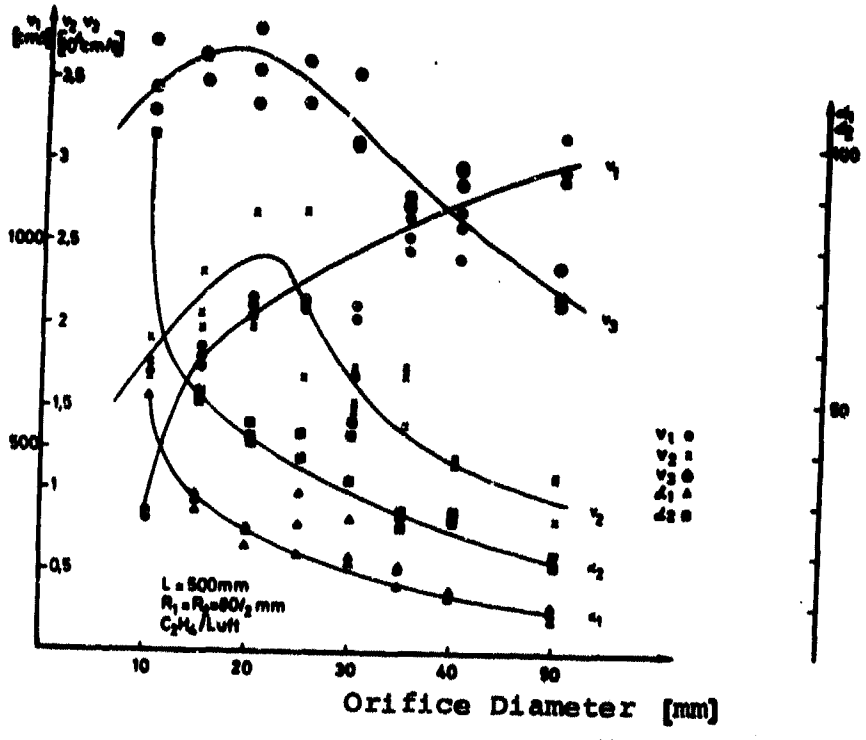

Fig. 12: Flame speed and α up and downstream of orifice for C_2H_4-air in 80/80 tube

The values of the flame speeds exhibit pronounced maxima for orifices of 20 - 25 mm diameter, corresponding to values of F_o/F_g of about 0.1. The apparent acceleration factors α, the ratios $V_3/V_1 = \alpha_3$ and $V_2/V_1 = \alpha_2$ increase continuously

towards smaller orifice diameters and decrease only very close to the critical diameters. This figure also demonstrates that the scatter of the data in different experiments is rather large.

Values for α in tubes of other diameter and for other mixtures fall approximately on one curve when they are plotted as a function of F_o/F_g (see Figure 13)

PRESSURE MEASUREMENTS

Another indication for the combustion intensity can be obtained from pressure measurements in the upstream an in the downstream section of the tube. Some typical pressure records are shown in Figure 14 (for different orifice diameters). In the driver section, the pressure increases and reaches a nearly constant value which depends on the ratio F_o/F_g. When the combustion process passes through the orifice a strong pressure rise occurs in the downstream section of the tube which can also be realized in the driver section after a short delay.

As to be expected, the maximum downstream pressure is again a function of F_o/F_g and depends on the diameter ($2R_2$) of the downstream tube diameter. This is demonstrated in Figure 15. For wide downstream tubes the pressure maxima occur close to the maxima of the flame speeds. The highest pressures are obtained for values of $2R_2$ which are about 2 to 2.5 times as large as the diameters of the driver section. This is demonstrated in Figure 16. For large downstream tubes (2R = 300 mm is close to unconfined), the peak pressures become rather low.

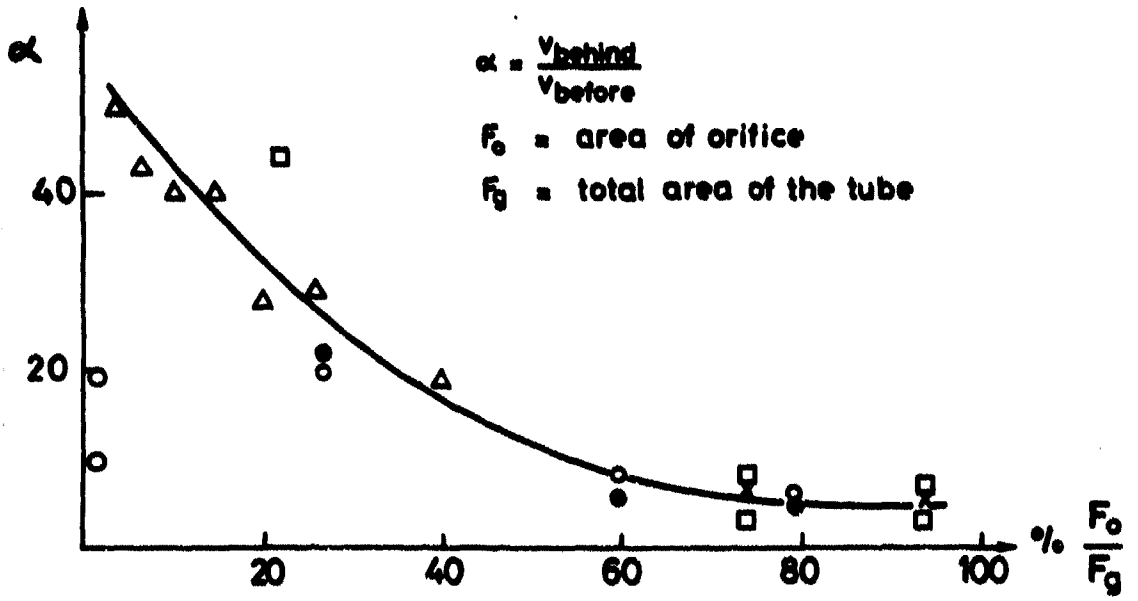

Fig. 13: Acceleration factor α for various open area ratios F_o/F_g for 40mm and 80 mm ignition section

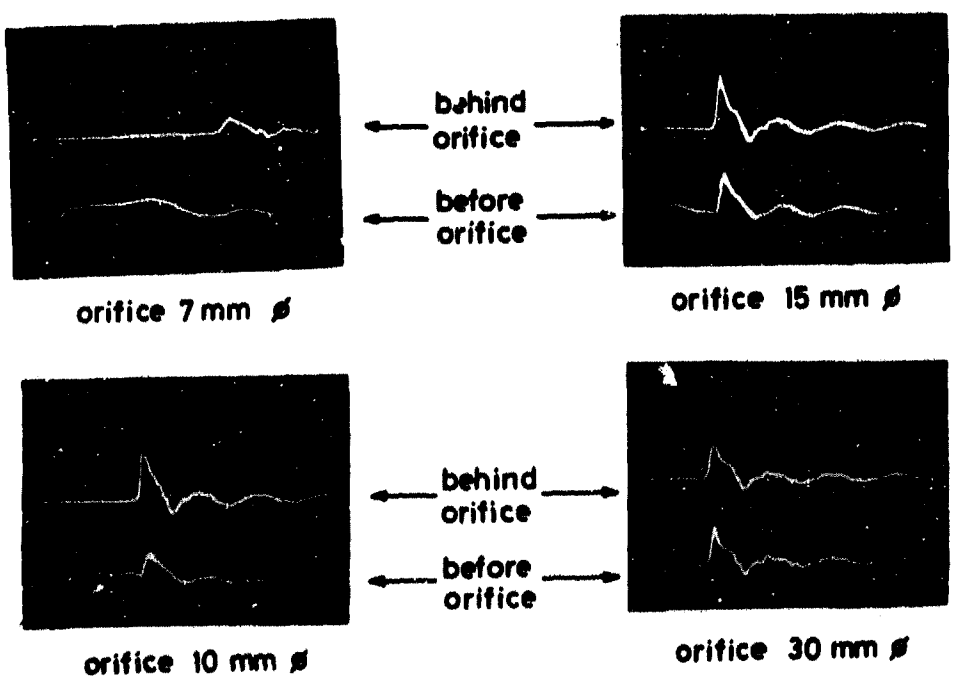

Fig. 14: Pressure profiles for C_2H_4-air mixture

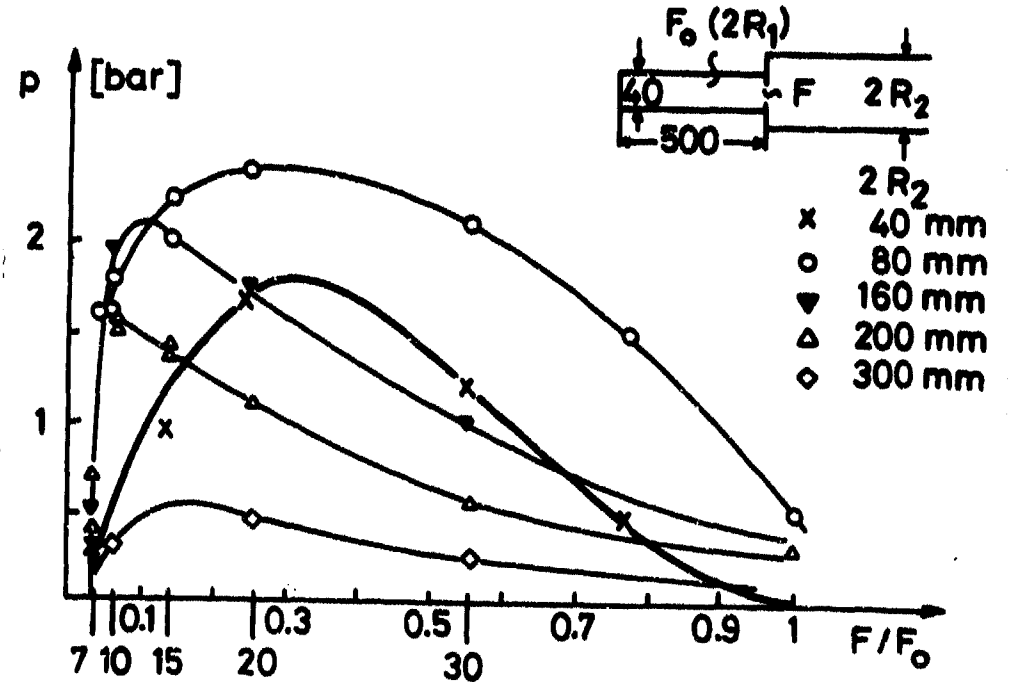

Fig. 15: Pressure behind orifice as a function of F/F_o for various tube combinations (C_2H_4-air)

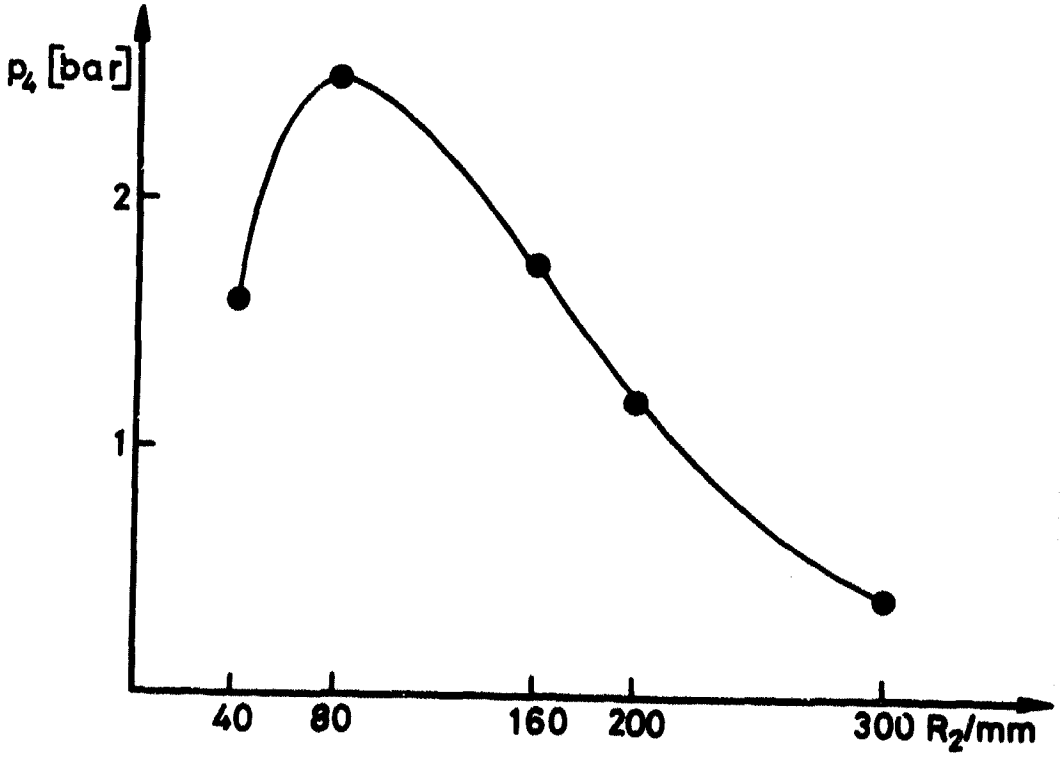

Fig. 16: Pressure downstream of orifice with diameter $2R_2$ ($2R_1$ = 40 mm; C_2H_4-air)

DISCUSSION

The flow through the orifice is generated by the flame moving along the tube. The pressure rise in the driver section is determined by this flame and the flow through the orifice. In a closed tube the increase of pressure is determined by

$$\frac{d}{dt}\left(\frac{P}{P_o}\right) = \frac{\Lambda \cdot \alpha_f \cdot F_g}{V_o} \gamma \frac{\Delta H}{C_p T_o} \left(\frac{P}{P_o}\right)^{\frac{1}{\gamma}}$$

P_o = initial pressure

P = Pressure at time t

F_g = cross section of the tube

Λ = Flame velocity relative to the unburned gas

α = Flame area factor

γ = ratio of specific heats

C_p = mean specific heat

T_o = initial temperature

$V_o = F_g \ell$ = volume of the tube

If gas is released through an orifice oposite to the ignition spark, the flow through the orifice has the velocity

$$w = \sqrt{2 \frac{\gamma}{\gamma-1} \frac{P}{\rho} \left(1 - \left(\frac{P_o}{P_1}\right)^{\frac{\gamma-1}{\gamma}}\right)}$$

The mass flux is given by

$$\dot{m} = F_{eff} \left(\frac{P}{P_o}\right)^{\frac{1}{\gamma}} \sqrt{\frac{\gamma}{\gamma-1}\left[1 - \left(\frac{P}{P_o}\right)^{\frac{\gamma-1}{\gamma}}\right]} \sqrt{2P\rho}$$

Here F_{eff} is the effective area which includes effects of friction and flow contraction. It can be calculated from the orifice area F_o with $F_{eff} = F_\phi \cdot a_6$ where a_6 can be calculated from the empirical relation

$$a_6 = 0.598 + 0.4 \left(\frac{F_o}{F_g}\right)^2 .$$

$(F_o/F_g \leq 0.7)$

Using this expression for the flow through the orifice, the change of pressure, neglecting heat losses, can be approximated by

$$\frac{d}{dt}\left(\frac{P}{P_o}\right) = \frac{\Lambda \alpha_1 F_o}{V_o} \gamma \frac{\Delta H}{C_p T_o} \left(\frac{P}{P_o}\right)^{\frac{1}{\gamma}} - F_{eff} \frac{\gamma\sqrt{2}}{\sqrt{\gamma-1}} \frac{C_o}{V_o} \left(1 + \frac{\Delta H}{C_p T_o}\left(\frac{P_o}{P}\right)^{\frac{\gamma-1}{\gamma}}\right) \cdot \left(\frac{P}{P_o}\right)^{\left(\frac{3}{2} - \frac{1}{2\gamma}\right)} \sqrt{1 - \left(\frac{P_o}{P}\right)^{\frac{\gamma-1}{\gamma}}}$$

(Subsonic flow in the orifice, C_o = sound velocity of the fresh unburned gas, Pressure = constant along the tube) An essential parameter which determines the pressure rise and therefore the speed of the jet is

$$\frac{\Lambda \alpha_1}{C_o} \cdot \frac{\Delta H}{C_p T_o} \cdot \frac{F_g}{F_{eff}} .$$

It contains the ratio fo F_o/F_g, in agreement with the experimental results reported.

The pressure measurements in the driver section indicated that after some time the pressure there becomes approximately constant (while $\Lambda \alpha_1$ change as to be observed from movie pictures). These pressure values have been used to calculate flow velocity w, mass flow $\dot{m}$ and momentum flux of the jet $\dot{m}w$ for a 40 mm tube and different orifice diameters. This is shown in Figure 17 together with the outside flame speed v_2 and the maximum

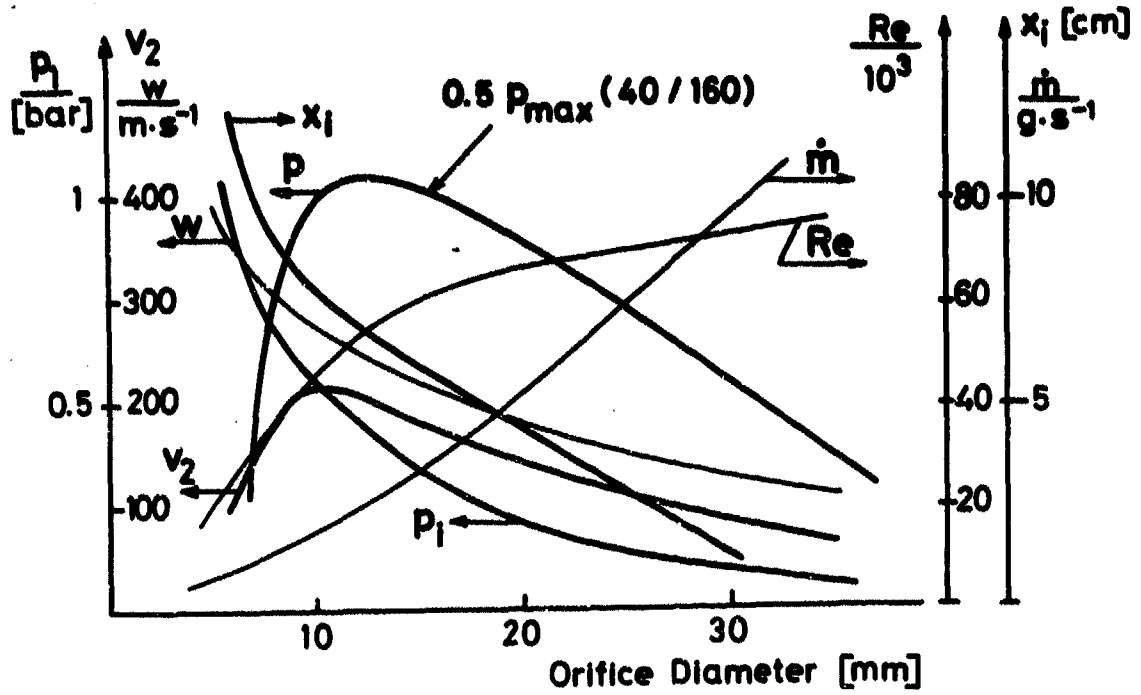

Fig. 17: Measured maximum pressure P in the ignition section for various orifice diameters. Reignition distance X_1 and flame speed downstream of orifice v_2 for a 40 mm diameter driver section. P_{max} is maximum pressure downstream.
The quantities: w = flow speed through orifice, Re and $\dot{m}$ are calculated for unburned gas grom measured values of P.

pressures measured downstream of the orifice for two different tube diameters $2R_2$. In addition the "reignition distance X_1" is plotted.

For orifices larger than 10 mm, the flame speed v_2 and the flow speed of the unburned gas in the orifice w run approximately parallel. This indicates that the flow of the highly turbulent unburned gas in the jet is an essential component for the high flame velocity. The mass of this gas increases with increasing orifice diameter. It is later on pushed further by the higher speed of the burned gas ($w_{2000} \approx 2.6 \quad w_{300}$, $\dot{m}_{2000} = 0.35\ \dot{m}_{300}$) flowing through the orifice.

Nozzle Flow

The flow speed of the unburned gas jet decreases with increasing (+Z) distance away from the jet approximately as

$$\frac{w_z}{w_o} = \frac{A\ d}{a + z}$$

where a is the "origin of similarity" of the jet and d the orifice diameter (see Fig. 18).

A typical distribution of the local axial velocity in Z direction is shown in Figure 18 ($Re_d \approx$ 15 000 - 30 000) for a 15°C and a 170°C jet. In addition the relative turbulence intensity u'_z/U_{zmax} is plotted, which amounts up to about 20%, a value which is not easily obtained in the main part of pipe flow. The radial distribution of turbulence intensity referred to the velocity of the axial center-line flow-velocity can be well described by a Gaussian distribution.

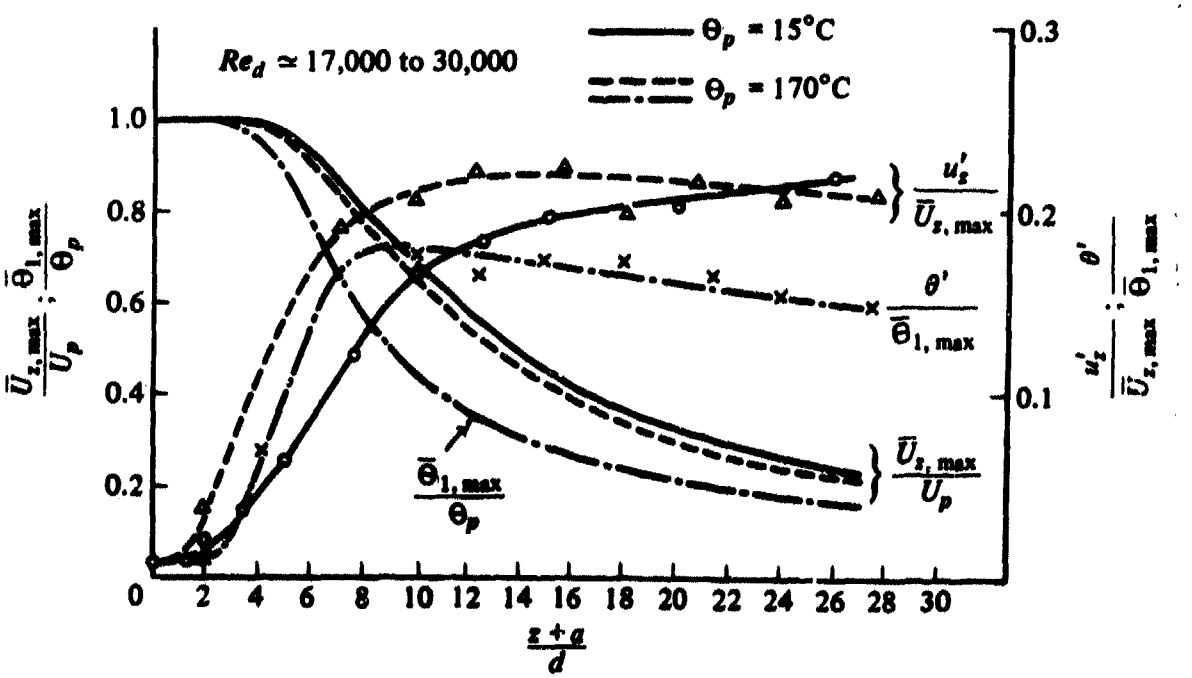

Fig. 18: Distribution of mean velocity, mean temperature, and relative intensities of axial velocity and temperature fluctuations along the axis of a round free jet. (Taking from Hinze, J.O.; Turbulence, McGraw-Hill, 1975)

For the eddy diffusion coefficient values of $\varepsilon_m = 0.0116\ U_p\ d$ are reported. For the spread of heat and matter values of $\varepsilon_g/\varepsilon_m \approx 1.3 - 1.4$ are obtained so that $\varepsilon_g \approx 0.016\ U_p d$ in the main part of the jet.

For a downstream tube diameter $2R_2 \gg 2R_1$, the jet is practically a free jet. If the diameter of the downstream tube is not large compared to the orifice diameter, the jet is no longer a free jet. The entrainment process will become different and a recirculation zone is generated.

Flame propagation through orifices

The values of w and Re in Fig. 17 are based on pressure measurements in a 40 mm diameter tube. It is probable that for larger tubes the absolute values of P and therefore w and the other calculated properties are somewhat different, the dependence on F_o/F_g, however, should remain similar.

Some values of ε_g for the conditions in Fig. 17 are given in the following table

w	280	180	130	m/sec
d	1	2	3	cm
ε_g	440	570	624	cm^2/sec
$\sqrt{\varepsilon_g}$	21	24	25	$cm/\sqrt{sec}$

For a laminar flame, the flame velocities is given by $\Lambda \sim \sqrt{\frac{D}{\tau}}$ where D is the molecular diffusion coefficient and τ the main reaction time. If D is replaced by ε_g (This seems reasonable as long as d is not too large), obtained for orifice flow, a strong increase of the local flame velocity would result in the unburned gas of the jet.

When the flame moves towards the orifice, a certain amount of the unburned gas from the driver section passes through the orifice before the flame reaches the orifice. The mass of unburned gas leaving the driver section increases with increasing orifice diameter (see Fig. 17). At the same time, the Reynolds number and ε_μ increase in the "jet" so that the local flame speed relative to the unburned gas should increase proportional to $\sqrt{\varepsilon_\mu}$.

As soon as the flame passes the orifice, it experiences high velocity gradients at the boundary of the jet. For large orifices it passes more or less disturbed through the orifice and its front velocity is now determined by the jet-plus the increased flame velocity, while its velocity perpendicular to the z direction depends on the local flow properties of the gas. At the same time, the hot gases pass the orifice and push the flame with the higher velocity of the hot jet.

If the orifice becomes narrower, a reignition distance X; can be observed, which for the experiments performed, seems to be proportional to the orifice diameter d (for the same F_o/F_g) and therefore to a certain extent mixing controlled. At first the flame front seems to break up into flame kernels (see Fig. 11). For still smaller orifices the flame first seems to be extinguished and reignited at a later stage. Now a jet of hot burned gas, which at least at the very beginning, flows with higher velocity (see above , $\dot{m} \cdot w$ remains the same) and entrains unburned gas. This mixing of burned and unburned gas generates zones with different fuel-air concentrations and temperatures such that high temperature corresponds to low fuel-air concentration and vice versa. This can generate self ignition or prepare zones which are on the way (radicals!) towards self-ignition, if they stay at the corresponding state for sufficiently long time. In addition, the flame velocity in such a mixture, as long as the fuel-air concentration is not too low increases with temperature. (Both effects become more important when the O_2 content is increased)

At a certain distance "reignition" takes place and the flame develops from this reignition center as a spherical flame with speeds close to 100 m/sec (see Fig. 9) (an indication for the strong entrainment of unburned gas into the hot jet). The center of this flame ball moves with jet speed and the combustion in +z and -Z direction cause a high apparent flame speed into z direction. This is also demonstrated by the maximum pressure values for a 40/160 tube combination (see Fig. 17). For still smaller orifice diameters, the jet volume decreases and therefore the highly turbulent volume where the local flame velocity is high, decreases, the rapidly exploding volume becomes smaller. This continus until towards smaller orifices entrainment becomes so rapid that the flame cannot reignite any more.

This is a qualitative description. For a quantitative description, which allows extrapolation to larger dimensions, further experiments have to be performed.